Research Article Vol. 3, No. 8 / 15 August 2020 / OSA Continuum 2175
OSA CONTINUUM

Complex shaping of the depth of focus

OMEL MENDOZA-YERO

Institut de Noves Tecnologies de la Imatge (INIT), Universitat Jaume I, 12080 Castelló, Spain
omendoza@fca.uji.es

Abstract: In this manuscript an exact solution to the inverse problem of axial beam shaping along the focus of a convergent lens is found. This allows to extend, within the framework of the scalar theory of diffraction, the mathematical formalism of complex pupils to include axial phase modulation. Numerical simulations based on Fourier transform as well as convolution operations indicate that amplitude and phase modulation can be performed simultaneously. It is also shown that include or not phase modulation in the beam shaping process can increase its efficiency more than three times. In addition, an analytical expression for the Gouy phase that depends on the introduced phase modulation was also derived. It is expected that obtained results benefit many photonic applications involving the control and manipulation of light along the focal region.

1. Introduction

Properly designed optical pupils can be used to engineer the light distribution at the focal region. Several efforts to achieve full control over amplitude, phase and polarization of light focused with high numerical aperture objective lenses have been carried out [1–4]. Furthermore, within the framework of the scalar theory of diffraction some alternative focal beam shaping methods, valid under the paraxial approximation, have also demonstrated their usefulness in many practical applications [5–7]. Several types of pure amplitude pupils were used to increase the depth of focus and/or control the distribution of light near the focus. On this point, among other proposals one can find spatial filters based on the definition of Strehl irradiance ratio [8], specific apodizers applied upon zone plates that generate multiple foci [9], the cascade of two binary phase diffractive optical elements [10], or the combination of diffractive grating and a binary diffractive lens [11]. With similar purposes, phase-only optical elements have been employed to get axial super-resolving imaging [12] or extend the depth of focus through different strategies that include, but are not limited to an optimization design method [13], an adaptive-optic loop working as a dynamic programmable phase-only filters [14] or specific designed diffractive optical elements (DOEs) like the so-called peacock eye DOE [15] and light sword lens [16,17], which were recently proposed for ophthalmic presbyopia compensation.

In general the design of optical pupils for approaching the field amplitude near the focus depends on the solution of an inverse problem. That is; starting from a three-dimensional distribution of light around the focal region one should be able to find the most suited optical element that once placed at the pupil plane fits the expected field amplitude. This is a highly challenging task because axial and transversal irradiance profiles cannot be tailored separately, but one influences the shape of the other. Even so depending on the application users might be more interested in a particular type of beam shaping. For instance, in surface microprocessing of materials i.e., for texturing or cleaning, the transverse rather than the axial shape of the laser irradiance is usually more important. In contrast, for applications including beam focalization for volumetric ablation of transparent objects, or supercontinuum generation and filamentation, axial beam shaping is what really matters. In the latter case, it is known that Fourier transform (FT) formalism gives us a powerful tool to calculate the complex pupil functions corresponding to the inverse problem [18]. Hence, the beam shaping can be carried out with relative high-accuracy and low computation time at the expense of using complex pupils that cannot be directly encoded

#400238 https://doi.org/10.1364/OSAC.400238
Journal © 2020 Received 16 Jun 2020; revised 17 Jul 2020; accepted 18 Jul 2020; published 5 Aug 2020

OSA CONTINUUM

into single optical elements or devices. To overcome this limitation the designed complex pupils were implemented on two spatial light modulators (SLMs) to separately display the amplitude and phase contributions [19]. In this context, an early publication of an approximate method to encode complex functions with phase filters [20] allowed the amplitude of complex pupils to be encoded into first prototypes of twisted nematic liquid-crystal SLMs working in the phase-only configuration, but still having low spatial resolutions (640×480 pixels) [21,22]. At present, the FT formalism can benefit from both the current progresses in SLM technology as well as the increased number of reported techniques aimed to encode complex fields. In addition, to the best of my knowledge, axial beam shaping with complex pupils is currently limited to reproduce the amplitude of the desired electric field along the focus, without considering its phase content.

In this manuscript the theory of complex pupils is extended to include phase modulation. The implementation of the FT formalism with the double-phase encoding method [23] and high spatial resolution (1920×1080 pixels) phase-only SLMs is also discussed. Furthermore, the proposed beam shaping method is complemented with the analysis of aspects related to its efficiency and the associated Gouy phase. It is shown that the extended theory of complex pupils allows performing not only amplitude but also phase shaping of the focus in the axial direction, simultaneously. In this context, the double-phase method ensures a high accurate reconstruction of the complex pupils at the input plane of the focusing element. The designed complex pupils composed of circularly symmetric masks are calculated from a direct (non-iterative) fast Fourier transform (FFT), and a rescaling process. In addition, the potential of the FT formalism for carrying out the dynamic spatial shaping of the focal region is shown by means of a couple of visualizations. Numerical simulations were used to corroborate all theoretical results. Accordingly, several electric fields having desired amplitude and phase profiles with different depth of focus were numerically reconstructed, achieving root mean squared errors (rmse) less than 10% in all cases. Additionally, the effects of axial beam shaping on the three-dimensional distributions of light at the focal region are also shown.

2. Theory of complex pupils using the double-phase method

In the scalar theory of diffraction, the focused electric field $E^{\circ}(z, R)$ near the Fourier plane of a convergent lens of focal length f and radius a can be determined by means of the Fresnel diffraction integral written in polar coordinates as follows

$$E(z, R) = \frac{k}{iz} \int_0^a p(r) e^{-i\frac{kr^2}{2f}} e^{i\frac{kr^2}{2z}} J_0\left(\frac{krR}{z}\right) r dr \tag{1}$$

In Eq. (1), the plane wave term e^{ikz} was considered as $E^{\circ}(z, R) = E(z, R)e^{ikz}$, where $E(z, R)$ is simple the electric field without the phase of the plane wave. The axial and radial coordinates near the focus are given by z and R, respectively. In addition, J_0 represents the Bessel function of the first kind of order zero, $k = 2\pi/\lambda$, where λ is the wavelength of an incident monochromatic uniform wave. In the thin lens approximation, the quadratic exponential term $kr^2/2f$ holds for the phase of the convergent lens with an axially symmetric complex pupil $p(r)$ defined within the interval $r \in [0, a]$, being $p(r) = 0$ outside this interval. If we restrict our analysis to pupils $p(s)$ that depend on the squared radial coordinate $s = r^2/a^2 - 1/2$, where $s \in [-1/2,\ 1/2]$, the electric field $E(z, R)$ in the axial direction ($R = 0$) can be reduced to the expression

$$E(\xi) = \frac{2\pi}{i}(\xi + \xi_0) e^{i\pi\xi} \int_{-\frac{1}{2}}^{\frac{1}{2}} p(s) e^{i2\pi\xi s} ds \tag{2}$$

In Eq. (2) the variable $\xi = a^2/(2\lambda z) - \xi_0$, and the constant $\xi_0 = a^2/(2\lambda f)$. Now, after multiplying left and right parts of Eq. (2) by the term $ie^{-i2\pi v\xi} e^{-i\pi\xi}/[2\pi(\xi + \xi_0)]$, where $v \in [-1/2,\ 1/2]$,

OSA CONTINUUM

and integrating over ξ to infinity one can get to the expression

$$p(v) = \frac{i}{2\pi}\mathcal{F}^{-1}\left\{\frac{E(\xi)e^{-i\pi\xi}}{(\xi+\xi_0)}\right\} \tag{3}$$

The result shown in Eq. (3) can be regarded as an exact solution to the inverse problem related to the axial beam shaping along the focus of a convergent lens. The symbol $\mathcal{F}^{-1}\{\ \}$ denotes the inverse FT operation. Note that to obtain Eq. (3) no approximations or assumptions have been made. Consequently, from a desired electric field $E(\xi)$ one can fully determine the complex pupil $p(v)$, so also $p(r)$ able to optically reconstruct this field near the focus. Here, it should be emphasized that beam shaping based on Eq. (3) is not limited to the amplitude of $E(\xi)$, but also includes its phase content. At this point, the complex field is conveniently expressed as $E(\xi) = -2\pi i\Lambda_{des}(\xi)e^{i[\pi\xi+\Theta_{des}(\xi)]}$, where $\Lambda_{des}(\xi)$ and $\Theta_{des}(\xi)$ hold for the desired amplitude and phase functions which are subject to be shaped. Then, after the substitution of $E(\xi)$ into Eq. (3) the codification of the linear phase term $-ie^{i\pi\xi}$ within $p(v)$ can be avoided

$$p(v) = \mathcal{F}^{-1}\left\{\frac{\Lambda_{des}(\xi)e^{i\Theta_{des}(\xi)}}{(\xi+\xi_0)}\right\} \tag{4}$$

From Eq. (4), the complex pupil $p(v)$, expressed in the squared radial coordinate v, is calculated by the one-dimensional inverse Fourier transform of the electric field $\Lambda_{des}(\xi)e^{i\Theta_{des}(\xi)}$ divided by $\xi+\xi_0$. It can be easily verified that the term $\xi+\xi_0$ compensates for a linear decrease in the amplitude $\Lambda_{des}(\xi)$ along the direction of propagation of the laser beam. To obtain the pupil function in the linear coordinate r a rescaling process $p(v) \rightarrow p(r)$ that consists of a numerical interpolation is carried out. Further details of this process are given in the next section. Here, one might realize that the beam shaping method depends on the ability to encode the complex pupils $p(r)$. In this manuscript the double-phase method [23] is used to encode these pupils into a phase-only SLM and optically reconstruct them at the input plane of the convergent lens. Hence, retrieved pupils $p_{ret}(x,y)$ expressed in the Cartesian coordinates x, y are given by the expression [23]

$$p_{ret}(x,y) \cong p\left(-\frac{x}{Mag},-\frac{y}{Mag}\right) \otimes \mathcal{F}\{P(f_x,f_y)\} \tag{5}$$

In Eq. (5), the term Mag holds for the magnification of the 4f imaging system (please, see Fig. 1), whereas the symbol $\otimes$ represents the convolution operation. Therefore, the optical reconstruction is exact except for a small loss of spatial resolution caused by the convolution of $p(x,y)$ with the FT of the spatial filter $P(f_x,f_y)$ expressed in the coordinates f_x, f_y of the frequency space. In practice, as the period δ of the sampling gratings used in the double-phase method is the lowest, for most commercially-available phase-only SLMs the spatial frequency separation $1/\delta$ between zero and first diffraction orders should be great enough to neglect the effects of this convolution.

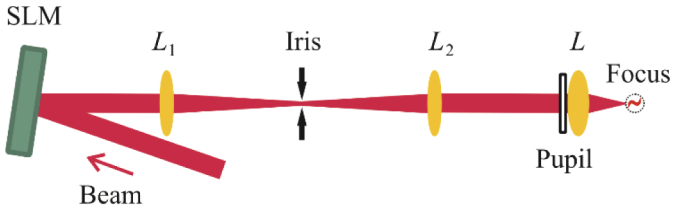

Fig. 1. Optical setup utilized to perform the axial beam shaping of the focus associated with a convergent lens L. The filtered 4f imaging system composed of lenses L_1 and L_2 is used to optically reconstruct the complex pupil at the input plane of the lens L.

OSA CONTINUUM

3. Numerical simulations of complex beam shaping

In this section the theory of complex pupils discussed above is corroborated by means of numerical simulations. These simulations describe the behavior of the optical system shown in Fig. 1 whose optical components and/or parameters are summarized below. A uniform wave with central wavelength of 800 nm impinges onto a phase-only SLM (with spatial resolution $1920x1080$ pixels, and pixel width 8 μm). The reflected light travels through a 4f imaging system composed of a couple of identical convergent lenses L_1 and L_2 of focal lengths $f_1 = f_2 = 1\ m$. The phase element $\alpha(x, y)$ used to encode a given complex pupil is sent to the SLM. The imaging system forms a filtered image of $\alpha(x, y)$ at the pupil plane of an ideal (free from optical aberrations) convergent lens L of focal length $f = 50\ mm$. The filtering process is carried out with a circular iris of radius $\varepsilon = f\lambda/\delta$ located at the Fourier plane of the optical imaging system. The radius ε coincides with the distance from the propagation axis to the first diffraction order of the above-mentioned sampling gratings. Each phase element $\alpha(x, y)$ is computer generated following the procedure described below.

It starts with the definition of the desired amplitude and phase functions $\Lambda_{des}(\xi)$ and $\Theta_{des}(\xi)$. Each of these functions are sampled with N_1 points determined from the absolute value of $\xi(z_{ini}) - \xi(z_{end})$, where the axial positions $z_{ini} = f - \Delta z/2$, $z_{end} = f + \Delta z/2$, and Δz is the depth of focus. The term $1/(\xi + \xi_0)$ is also sampled with N_1 points and multiplied by the function $\Lambda_{des}(\xi)$. Then a couple of vectors of $N_2 = 541$ points are digitally constructed. Their central N_1 points contain the sampled functions $\Lambda_{des}(\xi)$ and $\Theta_{des}(\xi)$, whereas the remaining points are zero. Before making the inverse FFT defined by Eq. (4), the amplitude and phase vectors are zero padded to longer vectors e.g., $N_3 = 100N_2$ points. Finally, the complex pupil $p(v)$ is calculated by downsampling the inverse FFT to N_2 points.

In the next step, the complex pupil $p(v)$ is rescaled to get the unknown function $p(r)$. To do that the interpolation algorithm associated with the MATLAB function interp1 is used. In Fig. 2 a representative example is given. It shows a complex pupil $p(s)$ designed to generate a focus with super-Gaussian amplitude $\Lambda_{des}(\xi) = e^{-\xi^\gamma/\sigma}$, where $\gamma = 8$, $\sigma = 10^{-3}$, and linear phase $\Theta_{des}(\xi) = \pi\xi$. In this example the depth of focus was $\Delta z = 3\ mm$. The amplitude and phase profiles of $p(v)$ are shown in Figs. 2(a) and 2(d), respectively. After rescaling, the corresponding profiles of $p(r)$ appear in Figs. 2(b) and 2(e), respectively. Owing to the rescaling algorithm both profiles were displaced and compressed toward the outer parts. Two-dimensional amplitude $A(x, y)$ and phase $\varphi(x, y)$ masks are computer generated after the azimuthal rotation of curves given in Figs. 2(b) and 2(e) around their origins as shown in Figs. 2(c) and 2(f), respectively.

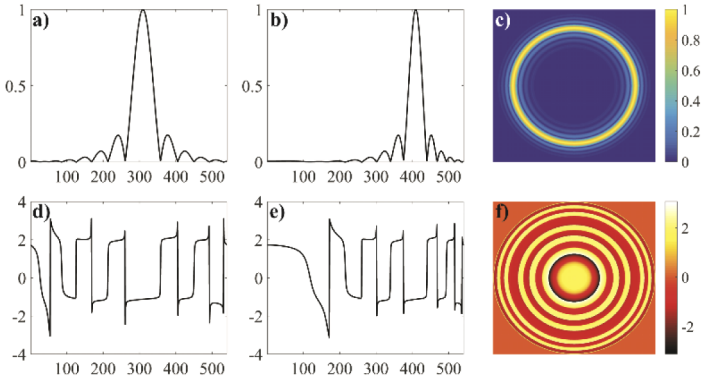

Fig. 2. Amplitude (a), (b) and phase (d), (e) masks of a complex pupil expressed in r^2 and r coordinates. This complex pupil generates a super-Gaussian amplitude with a linear phase at the focal region of a convergent lens.

OSA CONTINUUM

Then, the complex pupil $p(x, y) = A(x, y)e^{-i\varphi(x,y)}$ is encoded into a single-phase element $\alpha(x, y)$ by using the expression (4) of the double-phase method [23]. In Figs. 3(a), 3(b) and 3(c), the circularly symmetric masks $\theta(x, y)$ and $\vartheta(x, y)$ and $\alpha(x, y)$ for the example discussed above are shown. The phase element $\alpha(x, y)$ is defined within the interval $[-3\pi/2,\ \ 3\pi/2]$ so, a total phase range of 3π is needed for its implementation with a phase-only SLM. The 4f optical system described in Fig. 1 carries out the optical reconstruction of the complex pupil $p(x, y)$ in front of the convergent lens. This is done with a theoretical approximation given by Eq. (5). Consequently, at this plane instead of $p(x, y)$ one gets the retrieved pupil $p_{ret}(x, y)$ (or $p_{ret}(r)$ in polar coordinates).

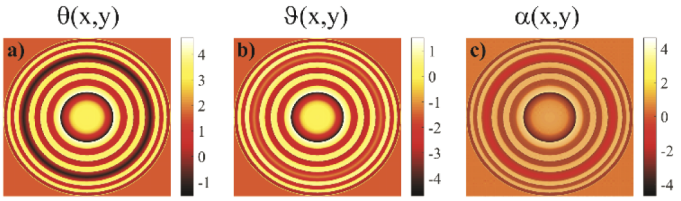

Fig. 3. Phase element $\alpha(x, y)$ used to encode the complex pupil $p(r)$. In accordance with the double-phase method $\alpha(x, y)$ is computer generated with the phase masks $\theta(x, y)$ and $\vartheta(x, y)$ corresponding to two uniform waves.

The accurate of the axial beam shaping is numerically tested by means of four user-defined electric fields with different depth of focus. For this purpose, the retrieved amplitude and phase profiles Λ_{ret} and Θ_{ret} assessed from a direct numerical evaluation of the Fresnel diffraction integral for $p(r) = p_{ret}(r)$ and $R = 0$, are compared with the desired amplitude and phase profiles Λ_{dis} and Θ_{dis}, respectively. The results are shown in Fig. 4. The desired electric fields are plotted with solid lines, whereas the retrieved ones are represented by circular points. The first electric field corresponds to the pupil shown in Fig. 2. It is composed of a super-Gaussian amplitude $\Lambda_{des}(\xi) = e^{-\xi^\gamma/\sigma}$, where $\gamma = 8$, $\sigma = 10^{-3}$, see Fig. 4(a), and a linear phase $\Theta_{des}(\xi) = \pi\xi$, see Fig. 4(b), with ($\Delta z = 3\ mm$, $N_1 = 15$). The second electric field has triangular amplitude profile $\Lambda_{des}(\xi) = 1 - |\xi|$, see Fig. 4(d), and the cosine phase $\Theta_{des}(\xi) = \pi\cos\pi\xi$, see Fig. 4(e), with ($\Delta z = 6\ mm$, $N_1 = 29$). For the third electric field, the amplitude profile $\Lambda_{des}(\xi) = \sin 2\pi\xi + \cos\pi\xi/2$, see Fig. 4(g), and a cubic phase $\Theta_{des}(\xi) = \pi\xi^3$, see Fig. 4(h), with ($\Delta z = 9\ mm$, $N_1 = 43$) are selected. In the last example, all previously defined amplitude and phase profiles are included in a unique electric field that forms three different foci of similar characteristics, simultaneously. It means that, one single complex pupil is employed to synthetize three different foci, each one having a different amplitude and phase pattern. In this last example all foci were designed with $\Delta z = 4\ mm$ and $N_1 = 19$. In order to have desired phase functions defined within the phase range of the SLM, the variable ξ was sampled within the interval $\xi \in [-1,\ 1]$ with N_1 points. To do that, $\xi = \xi/\xi_{ave} - min(\xi/\xi_{ave}) - 1$, where ξ_{ave} is the mean value of ξ between the points $z = z_{ini}$ and $z = z_{end}$, whereas the function *min* yields the minimum value.

After a visual inspection of these curves it is apparent that desired and retrieved profiles are very close. In fact, the calculus of the rmse gets values [0.79 %, 0.55 %], [0.53 %, 3.3 %] [1.73 %, 3.99 %] and [4.42 %, 7.71 %] for the amplitude and phase profiles, respectively. Small discrepancies are mainly due to the limited number of N_1 points used to sample the desired functions. If the selected depth of focus Δz is great enough to guarantee full recovery of desired functions after simple interpolation, beam shaping should be done with low values of rmse. As a rule of thumb for a fixed set of optical components and light parameters a, f, λ, those values of Δz such that $N_1 \geq 15$ should give low rmse e.g., below 10%. It is also expected that rmse increases when increasing of the complexity of desired functions.

OSA CONTINUUM

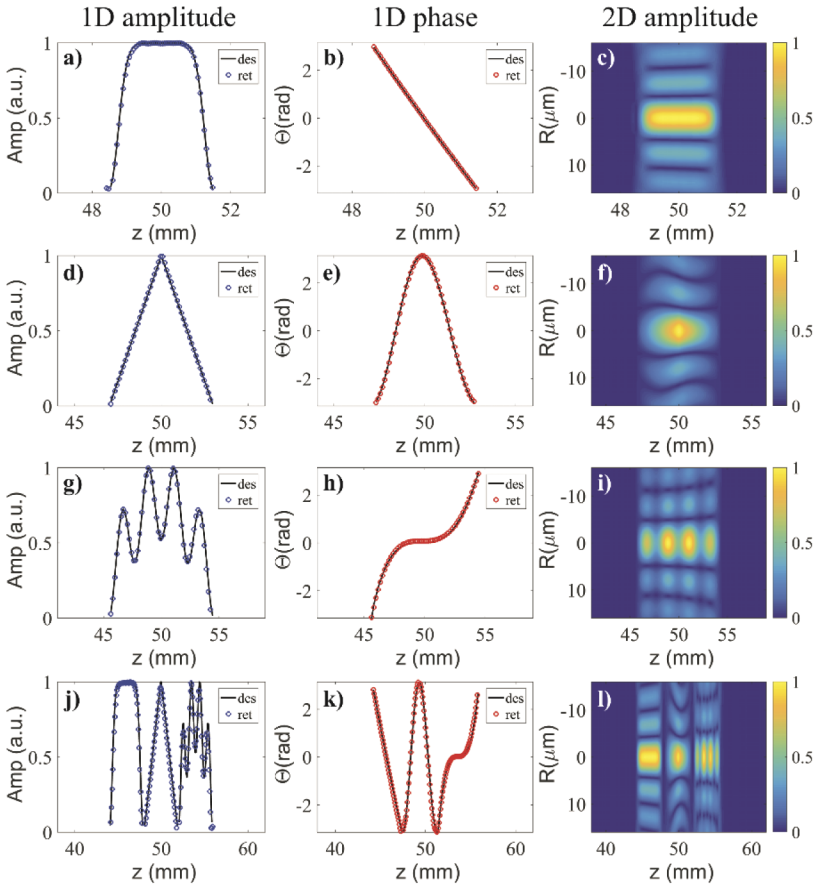

Fig. 4. Comparison between retrieved (circle symbols) and desired (solid lines) amplitude and phase distributions of light near the focus of a convergent lens. In the right part, corresponding two-dimensional amplitude fields are included.

The results shown in Fig. 4 corroborate the extended theory of complex pupils discussed above. Furthermore, in the right-part of Fig. 4 appears the two-dimensional normalized amplitude fields calculated by means of Eq. (1) for $p(r) = p_{ret}(r)$, but this time $R \neq 0$, please see Figs. 4(c), 4(f), 4(i), and 4(l). As it can be noted axial beam shaping also influences the transversal distribution of light along the focal region. In particular, the spatial shape of transversal amplitude patterns depends on the axial phase $\Theta_{ret}(\xi)$. This type of amplitude-phase coupling could be used to make a rough estimation of the axial phase along the focus by raster scanning measurements of the transversal irradiance using a typical CCD or CMOS camera.

Now the suitability of complex beam shaping for the dynamic management of the focused light is illustrated with the help of two visualizations shown in Fig. 5. Each movie was edited from a set of 50 pre-calculated phase masks $\alpha(x, y)$ stored in the computer's memory. For this simulation two similar sets of complex pupils were calculated. The first one generates a variable light filament with constant phase along the propagation direction of the laser beam. These filaments were synthetized from the functions $\Lambda_{des}(\xi) = e^{-\xi^{\gamma}/\sigma}$ and $\Theta_{des}(\xi) = 0$, varying the depth of focus in the range $2\ mm \leq \Delta z \leq 20\ mm$, see Visualization 1. For the second movie the constant phase was substituted by the sinusoidal function $\Theta_{des}(\xi) = \pi \sin 3\pi\xi$ with $\xi = [-1,\ 1]$, but the amplitude function $\Lambda_{des}(\xi)$ and the depth of focus Δz remain the same, see Visualization 2.

OSA CONTINUUM

For completeness, the corresponding two-dimensional normalized amplitude field is also shown at the top-part of each visualization. From these movies one can realize the potential of the method to dynamically modify both the amplitude and phase of the electric field, simultaneously. Owing to the relative fast evaluation of Eq. (4) by using the direct FFT the maximum shaping velocity depends on the refresh rate of the liquid crystal display which is basically determined by the speed of the control electronics. The refresh rate of phase-only SLMs are typically from 60 Hz up to 200 Hz but after improving their dynamic response [24] it can be increased up to few kHz, or even in excess of GHz when applying novel architectures [25]. In addition, the absence of iterative Fourier-transform algorithms (e.g. Gerchberg–Saxton's or Fienup's method) may allow faster-enough operations to deal with certain beam shaping applications in real time. In this context it was also found that the amplitude full-width-at-half-maximum of the longest light filament achieved for $\Delta z = 20$ *mm* is increased 67 times with respect to that of the axial Airy pattern.

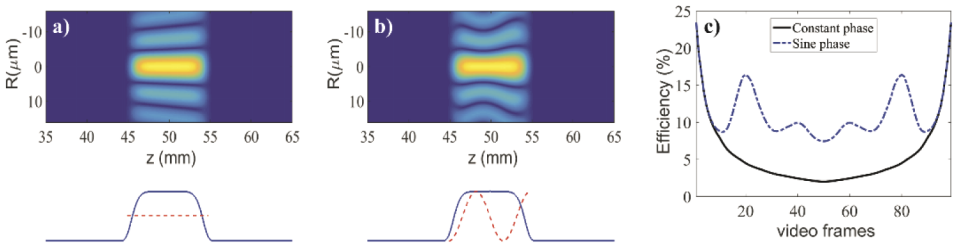

Fig. 5. Examples of dynamic axial beam shaping. Light filaments with variable depth of focus and constant phase (see Visualization 1) or sinusoidal phase (see Visualization 2). In the right part, the comparison of efficiency between the constant phase case (solid line) and sinusoidal one (dotted line) is shown.

Another important aspect to consider is the efficiency of the axial beam shaping. Here, the efficiency η was evaluated by the ratio $\eta = I_{ret}/I_{cir}$ between axial irradiances originated by a complex pupil ($I_{ret} = |A_{ret}|^2$), and a circular aperture of radius a ($I_{cir} = |A_0 \mathrm{sinc}\xi|^2$, where A_0 is a constant). For above visualizations, the evolution of this parameter with video frames shows values below 25% in all cases. In the Visualization 1, as the depth of focus becomes longer the efficiency abruptly decreases from $\eta = 23.4$ % ($\Delta z = 2$ *mm*) up to $\eta = 2.0$ % ($\Delta z = 20$ *mm*). In contrast, with the introduction of phase modulation in the light filament (see Visualization 2) the efficiency of the diffracted light was increased. Specifically, for the two absolute maxima of the sine phase curve located at frames 20 and 80 the efficiency changes from 4.5% (constant phase curve) to 16.4% (sine phase curve), which is more than 3 times the efficiency without phase modulation. This fascinating behavior is originated by the change in the transmittance of the complex pupil due to the introduction of phase modulation in the focus. To clarify this point, one-dimensional complex pupils used to obtain constant and sinusoidal phase modulation are shown in Figs. 6(a), 6(b), 6(e) and 6(f), respectively. Note that, although both complex pupils generate equal on-axis light filaments, please see two-dimensional field amplitudes in Figs. 6(d) and 6(h), their transmittances are clearly different. To emphasize this fact, corresponding two-dimensional amplitude masks are shown in Figs. 6(c) and 6(g). The calculus of the ratio between transmittances of these masks yields 3.4, which justify the increasement of the efficiency reported before.

On the other hand, the phase modulation along the axial focus is related to the well-known Gouy phase [26,27], defined as the difference between the phase of the electric field and that of a plane wave with the same wavelength. Hence, as the plane wave term e^{ikz} was taken into account in Eq. (1) by the expression $E^{\circ}(\xi) = E(\xi)e^{ikz}$, the Gouy phase $G(\xi)$ due to electric fields in the

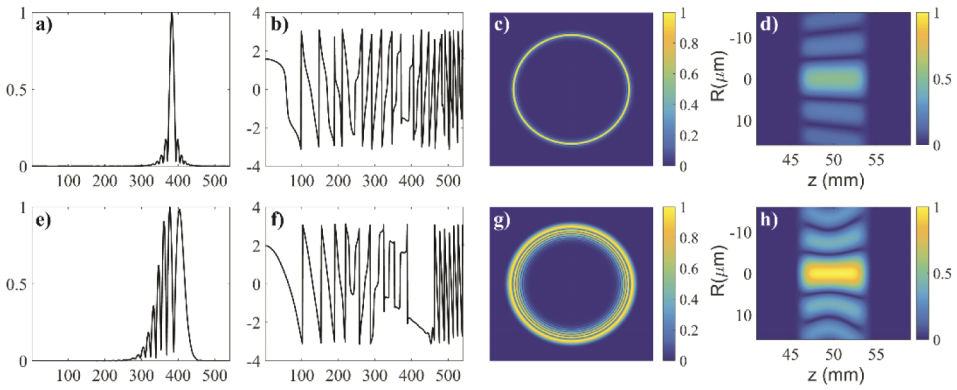

Fig. 6. Comparison of two complex pupils that generate the same on-axis super-Gaussian amplitude, but different phase modulation along the focus. One-dimensional amplitude and phase profiles (a), (b), (e), and (f) for the constant and sinusoidal phase modulation cases, respectively. Corresponding two-dimensional amplitude masks (c) and (g) as well as the field amplitudes (d) and (h) around the foci and normalized to the second case are also shown.

form $E^{\circ}(\xi) = 2\pi\Lambda_{des}(\xi)e^{i[\pi\xi+\Theta_{des}(\xi)-\pi/2+kz]}$ can be written as

$$G(\xi) = \pi\xi + \Theta_{des}(\xi) - \pi/2 \tag{6}$$

The additive phase term $\pi\xi$ in Eq. (6) is common to all solutions of Eq. (1) discussed in this manuscript. It changes from positive to negative values when light passes through the focus. So, within the axial interval defined from $z_{ini} = f - \Delta z/2$ to $z_{end} = f + \Delta z/2$, the focused light acquires a Gouy phase shift that can be determined by $G(\xi_{end}) - G(\xi_{ini})$, where $\xi_{end} = a^2/(2\lambda z_{end}) - \xi_0$ and $\xi_{ini} = a^2/(2\lambda z_{ini}) - \xi_0$. This Gouy phase shift increases when increasing the depth of focus Δz, and does not depends on the amplitude functions $\Lambda_{des}(\xi)$. Phase discontinuities (or phase jumps) by an amount of π occur at zeros of $\Lambda_{des}(\xi)$. For instance, for a binary circular pupil of radius a the analytical solution for the electric field yields $E(\xi) = 2\pi e^{i(\pi\xi-\pi/2)}(\xi + \xi_0)[\sin(\pi\xi)]/(\pi\xi)$. Then, phase anomalies appear for $\xi = \pm n$, where $n = 1, 2, \ldots$ at the axial positions $z_{\pm} = f/(1 \pm 2n\lambda f/a^2)$. The Gouy phase calculated by Eq. (6) gives the set of values $G(\pm n) = (\pm 2n - 1)\pi/2$. In Fig. 7(a) the first six phase anomalies in the Gouy phase $G(\xi)$ are represented using the mod π function and the parameters $a = 1\ cm, f = 2\ cm$, and $\lambda = 632.8\ nm$. This coincides with a classical result reported in [27], please see Fig. 2 of this publication. In addition, at the focal position ($z = f$ and $\xi = 0$) $G(0) = -\pi/2$, and the symmetry property of Gouy phase $G(n) + G(-n) = -\pi$ is also fulfilled.

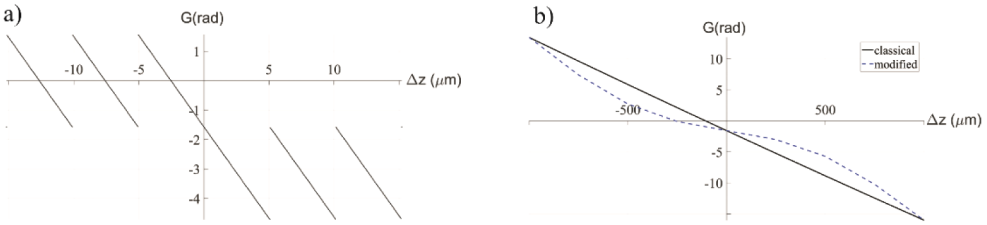

Fig. 7. Gouy phase associated with the beam shaping method. Classical Gouy phase provided by Eq. (6) due to a circular binary pupil placed in front of a convergent lens a), and Gouy phase due to the generation of a super-Gaussian amplitude along the focus with (dotted lines) and without (solid lines) phase modulation b).

OSA CONTINUUM

Equation (6) suggests that Gouy phase can be tuned due to the phase modulation originated by phase functions $\Theta_{des}(\xi)$, i.e., for $\Theta_{des}(\xi) = -\pi\xi$ one can compensate for the Gouy phase shift within the axial interval $[z_{ini},\ z_{end}]$. Another example is given in Fig. 7(b). Here, the Gouy phase for the electric field $E(\xi) = 2\pi e^{i(\pi\xi+\Theta_{des}(\xi)-\pi/2)}(\xi+\xi_0)e^{-\xi^\gamma/\sigma}$ with parameters $\gamma = 8$, $\sigma = 10^{-3}$, $\Delta z = 2\ mm$, $a = 4.3\ mm$, $f = 50\ mm$, and $\lambda = 800\ nm$ is represented for two different situations. The first one (plotted with solid lines) corresponds to the classical case of $\Theta_{des}(\xi) = 0$, whereas in the second curve (plotted with dotted lines) $\Theta_{des}(\xi) = -\pi \sin \pi\xi$ with $\xi = [-1,\ 1]$. From the comparison of both curves the induced changes in the Gouy phase are apparent. Note also that as the amplitude term $2\pi(\xi+\xi_0)e^{-\xi^\gamma/\sigma}$ does not vanish, the Gouy phase shows no phase anomalies.

4. Conclusions

In this manuscript the theory of complex pupils is extended to include axial phase modulation within the focus. It is shown that Fresnel diffraction integral allows for an exact solution of the inverse focal shaping problem along the axial direction ($R = 0$). Electric fields with desired amplitude and phase profiles were encoded into circularly symmetric complex pupils calculated by a direct Fourier transform and a simple rescaling operation. The double-phase method was used to optically reproduce the complex pupils at the input plane of the convergent lens. This method ensures an almost exact reconstruction of the desired electric fields around the focus. Numerical simulations showed simultaneous amplitude and phase modulation of the focus by using representative functions having super-Gaussian, triangular or sinusoidal profiles and different depth of focus. The ability of the method for dynamic shaping was used to generate light filaments under controllable conditions. In this context, it was found that phase modulation can significantly increase the efficiency of shaping (more than three times in the present work). Furthermore, an analytical expression for the Gouy phase was also reported. It suggests that Gouy phase might be tailored in accordance with the shape of user-defined phase functions.

Apart from being limited to low numerical aperture focusing the main weaknesses of the proposed shaping method relies on the lack of accuracy to shape electric fields with axial dimensions in the order of the axial Airy pattern. That is; to reproduce the desired amplitude and phase functions with a minimum number of sampling points one cannot set the depth of focus below certain limit. This imposes a physical restriction to the method which is unable to shape a focus below this limit without increasing the rmse up to values that might not be assumed from a practical point of view. In contrast, this method has several strengths that can be briefly summarized as: it allows tailoring at will both the amplitude and phase of the focused light simultaneously, it is a direct rather than iterative beam shaping algorithm, it provides high accuracy generation of complex pupils and corresponding desired electric fields, it is based on the FT formalism that ensures a fast and dynamic focal shaping operation, and its practical implementation with the double phase method is straightforward. I believe that several photonic applications, including but not limited to laser material processing, generation and control of non-linear effects or light coupling into optical fiber can benefit from the proposed method.

Funding

Ministerio de Ciencia, Innovación y Universidades (PID2019-110927RB-100); Universitat Jaume I (UJI-B2019-37); Conselleria d'Educació, Investigació, Cultura i Esport (PROMETEO/2020/029).

Disclosures

The author declare no conflicts of interest.

OSA CONTINUUM

References

1. Z. Guan-Lin, G. Xu-Zhen, P. Yue, Z. Meng-Dan, W. Dan, Z. Hai-Han, L. Yongnan, T. Chenghou, and W. Hui-Tian, "Inverse method to engineer uniform-intensity focal fields with arbitrary shape," Opt. Express **26**(13), 16782–16796 (2018).
2. R. Guanghao, J. Chen, X. Wang, B. Gu, Y. Cui, and Q. Zhan, "Synthesis of focused beam with controllable arbitrary homogeneous polarization using engineered vectorial optical fields," Opt. Express **24**(21), 23667–23676 (2016).
3. J. Hao, Z. Yu, Z. Chen, H. Chen, and J. Ding, "Shaping of focal field with controllable amplitude, phase, and polarization," Chin. Opt. Lett. **12**(9), 090501 (2014).
4. K. Jahn and N. Bokor, "Intensity control of the focal spot by vectorial beam shaping," Opt. Commun. **283**(24), 4859–4865 (2010).
5. A. Möhl, S. Kaldun, C. Kunz, F. A. Müller, U. Fuchs, and S. Gräf, "Tailored focal beam shaping and its application in laser material processing," J. Laser Appl. **31**(4), 042019 (2019).
6. P. S. Salter and M. J. Booth, "Adaptive optics in laser processing," Light: Sci. Appl. **8**(1), 110 (2019).
7. Ó Martínez-Matos, P. Vaveliuk, J. G. Izquierdo, and V. Loriot, "Femtosecond spatial pulse shaping at the focal plane," Opt. Express **21**(21), 25010–25025 (2013).
8. J. Ojeda-Castañeda, L. R. Berriel-Valdos, and E. Montes, "Spatial filter for increasing the depth of focus," Opt. Lett. **10**(11), 520–522 (1985).
9. J. Ojeda-Castaneda and L. R. Berriel-Valdos, "Zone plate for arbitrarily high focal depth," Appl. Opt. **29**(7), 994–997 (1990).
10. B. Abdelhalim, M. Fromager, and K. Aït-Ameur, "Extended focus depth for Gaussian beam using binary phase diffractive optical elements," Appl. Opt. **57**(8), 1899–1903 (2018).
11. A. Motogaito, Y. Iguchi, S. Kato, and K. Hiramatsu, "Fabrication and characterization of a binary diffractive lens for controlling focal distribution," Appl. Opt. **59**(3), 742–747 (2020).
12. Z. Zalevsky, A. Shemer, A. Zlotnik, E. Ben Eliezer, and E. Marom, "All-optical axial super resolving imaging using a low-frequency binary-phase mask," Opt. Express **14**(7), 2631–2643 (2006).
13. F. Zhou, R. Ye, G. Li, H. Zhang, and D. Wang, "Optimized circularly symmetric phase mask to extend the depth of focus," J. Opt. Soc. Am. A **26**(8), 1889–1895 (2009).
14. B. Wattellier, C. Sauteret, J.-C. Chanteloup, and A. Migus, "Beam-focus shaping by use of programmable phase-only filters: application to an ultralong focal line," Opt. Lett. **27**(4), 213–215 (2002).
15. L. A. Romero, M. S. Millán, Z. Jaroszewicz, and A. Kolodziejczykd, "Double peacock eye optical element for extended focal depth imaging with ophthalmic applications," J. Biomed. Opt. **17**(4), 046013 (2012).
16. K. Petelczyc, A. Byszewska, E. Chojnacka, Z. Jaroszewicz, K. Kakarenko, A. Mira-Agudelo, A. Ostrowska-Spaleniak, A. Składowska, A. Kołodziejczyk, and M. Rękas, "The Light Sword Lens - A novel method of presbyopia compensation: Pilot clinical study," PLoS One **14**(2), e0211823 (2019).
17. K. Petelczyc, A. Kolodziejczyk, N. Błocki, A. Byszewska, Z. Jaroszewicz, K. Kakarenko, K. Kołacz, M. Miler, A. Mira-Agudelo, W. Torres-Sepúlveda, and M. Rękas, "Model of the light sword intraocular lens: in-vitro comparative studies," Biomed. Opt. Express **11**(1), 40–54 (2020).
18. C. W. McCutchen, "Generalized aperture and the three-dimensional diffraction image," J. Opt. Soc. Am. **54**(2), 240–244 (1964).
19. P. N. Gundu, E. Hack, and P. Rastogi, "High efficient superresolution combination filter with twin LCD spatial light modulators," Opt. Express **13**(8), 2835–2842 (2005).
20. J. A. Davis, D. M. Cottrell, J. Campos, M. J. Yzuel, and I. Moreno, "Encoding amplitude information onto phase-only filters," Appl. Opt. **38**(23), 5004–5013 (1999).
21. A. Márquez, C. Iemmi, J. C. Escalera, J. Campos, S. Ledesma, J. A. Davis, and M. J. Yzuel, "Amplitude apodizers encoded onto Fresnel lenses implemented on a phase-only spatial light modulator," Appl. Opt. **40**(14), 2316–2322 (2001).
22. J. A. Davis, C. S. Tuvey, O. López-Coronado, J. Campos, M. J. Yzuel, and C. Iemmi, "Tailoring the depth of focus for optical imaging systems using a Fourier transform approach," Opt. Lett. **32**(7), 844–846 (2007).
23. O. Mendoza-Yero, G. Mínguez-Vega, and J. Lancis, "Encoding complex fields by using a phase-only optical element," Opt. Lett. **39**(7), 1740–1743 (2014).
24. G. Thalhammer, R. W. Bowman, G. D. Love, M. J. Padgett, and M. Ritsch-Marte, "Speeding up liquid crystal SLMs using overdrive with phase change reduction," Opt. Express **21**(2), 1779–1797 (2013).
25. C. Peng, R. Hamerly, M. Soltani, and D. R. Englund, "Design of high-speed phase-only spatial light modulators with two-dimensional tunable microcavity arrays," Opt. Express **27**(21), 30669–30680 (2019).
26. P. Martelli, M. Tacca, A. Gatto, G. Moneta, and M. Martinelli, "Gouy phase shift in nondiffracting Bessel beams," Opt. Express **18**(7), 7108–7120 (2010).
27. X. Pang, D. G. Fischer, and T. D. Visser, "Generalized Gouy phase for focused partially coherent light and its implications for interferometry," J. Opt. Soc. Am. A **29**(6), 989–993 (2012).